Engineering Analysis with Boundary Elements 32 (2008) 811–823

Contents lists available at ScienceDirect

Engineering Analysis with Boundary Elements

journal homepage: www.elsevier.com/locate/enganabound

Regularity condition and numerical examination for degenerate scale problem of BIE for exterior problem of plane elasticity

Y.Z. Chen *, X.Y. Lin

Division of Engineering Mechanics, Jiangsu University, Zhenjiang, Jiangsu 212013, PR China

ARTICLE INFO

Article history:
Received 2 November 2007
Accepted 26 February 2008
Available online 21 May 2008

Keywords:
Regularity condition
Boundary integral equation
Exterior boundary value problem
Critical value for size
Non-trivial solution
Improper solution

ABSTRACT

This paper investigates the regularity condition at infinity in the exterior boundary value problem (EBVP) of plane elasticity. It is found that the usual suggested kernel, or the displacement from a fundamental field in textbooks on BIE, do not satisfy the regularity condition when the loadings on contour are not in equilibrium. A new kernel from a revised displacement expression in the fundamental field is suggested, which satisfies the regularity condition. In this paper, a numerical technique for evaluating the degenerate scale in boundary integral equation (BIE) is suggested. In the technique, the scale of a notch is changed gradually. Once the determinant for an influence matrix is nearly equal to zero, the degenerate scale is found. In addition, the eigenfunctions, or the non-trivial solutions, can also be evaluated. Three examples are presented to examine the results obtained from numerical solution of the BVP. In those examples, the relevant exact solutions are known beforehand. In the examination, a suggested kernel that satisfies the regularity condition is used. It is found that if the used size is near the critical value, the improper solution exists. However, if the used size is different from the critical value by 10%, a sufficient accurate numerical solution can be achieved.

1. Introduction

The boundary integral equation (abbreviated as BIE) was widely used in elasticity, and the fundamental for BIE could be found from Refs. [1–3]. Heritage and early history of the boundary element method was summarized more recently [4]. However, some difficult points for the BIE remain.

Some problems in the BIE may not be studied throughout. The first problem is about the regularity condition at infinity. It is known that the BIE for the exterior problem can be expressed in the following form:

$$\frac{1}{2}u_i(\xi)+\int_\Gamma P^*_{ij}(\xi,x)u_j(x)\,ds(x)=\int_\Gamma U^*_{ij}(\xi,x)p_j(x)\,ds(x)+D^*_{i(CR)}(\xi)\quad(i=1,2,\quad\xi\in\Gamma),\tag{1}$$

where the kernel $P^*_{ij}(\xi,x)$ has been defined in Ref. [3], and $U^*_{ij}(\xi,x)$ is obtained from the fundamental solution that may be differed each other by a rigid motion. In Eq. (1), the term $D^*_{i(CR)}(\xi)$ is defined by

$$D^*_{i(CR)}(\xi)=-\int_{CR}P^*_{ij}(\xi,x)u_j(x)\,ds(x)+\int_{CR}U^*_{ij}(\xi,x)p_j(x)\,ds(x)\quad(i=1,2,\quad\xi\in\Gamma),\tag{2}$$

where "CR" denotes a sufficient large circle. The regularity condition is defined by the equation $D^*_{i(CR)}(\xi)=0$. Alternatively speaking, if the equality $D^*_{i(CR)}(\xi)=0$ is satisfied, the regularity condition is fulfilled. We know that for a given stress field, the relevant displacements can be differed by three types of rigid motion. In the fundamental solution, any additional displacements in the type of rigid motion will influence the kernel $U^*_{ij}(\xi,x)$. Unfortunately, if the non-equilibrated loadings are applied on the contour and the usual kernel $U^*_{ij}(\xi,x)$ (available in any text book) is used, the terms $D^*_{i(CR)}(\xi)$ are not vanishing in general, or $D^*_{i(CR)}(\xi)\neq 0$, or the regularity condition is not satisfied. In this paper, the condition for $D^*_{i(CR)}(\xi)=0$ is considered in detail. It is found that if the fundamental field is expressed in pure deformable form, the regularity condition will be fulfilled (or $D^*_{i(CR)}(\xi)=0$). In this case, the terms $D^*_{i(CR)}(\xi)$ can be dropped from Eq. (1).

It was pointed out that the influence matrix of the weakly singular kernel (logarithmic kernel) might be singular for the Dirichlet problem of Laplace equation when the geometry is reaching some special scale [5]. In this case, one may obtain a non-unique solution. The non-unique solution is not physically realizable. From the viewpoint of linear algebra, the problem also originates from rank deficiency in the influence matrices [5].

The degenerate scale problem in BIE for the two-dimensional Laplace equation is studied by using degenerate kernels and Fourier series [6]. In the circular domain case, the degenerate scale problem in BIE for the two-dimensional Laplace equation is studied by using degenerate kernels and circulants, where the

* Corresponding author.
E-mail address: yizhou922@yahoo.com.cn (Y.Z. Chen).

0955-7997/$ - see front matter © 2008 Elsevier Ltd. All rights reserved.
doi:10.1016/j.enganabound.2008.02.004

ciculants means the influence matrices for the discrete system have a particular character [7]. By using a particular solution in the normal scale, the degenerate scale can be evaluated numerically [5].

In the case of plane elasticity, the degenerate scale problem in BIE still exists. For example, if the conventional boundary integral equation is used for a ring region with the vanishing displacements along the boundary, in some particular geometry condition the corresponding homogenous equation has non-trivial solution for the boundary tractions [8,9]. In fact, if the displacements are vanishing at the boundary of ring region, the stresses must also be equal to zero. Therefore, the obtained result seriously violates the basic property of elasticity.

In the case of $D^*_{i(\mathrm{CR})}(\xi)=0$, from Eq. (1) we can propose the following homogenous equation for the exterior problem:

$$\int_\Gamma U^*_{ij}(\xi,x)p_j(x)\,\mathrm{d}s(x)=0 \quad (i=1,2, \quad \xi\in\Gamma), \tag{3}$$

where Γ is the boundary of the notch, $\xi\in\Gamma$ is the source point, and $x\in\Gamma$ denotes the field point. Besides, the two kernels $P^*_{ij}(\xi,x)$ and $U^*_{ij}(\xi,x)$ can be found in textbook. It is seen that $p_j(x)=0$ is a trivial solution for the homogenous equation. As in the case of Laplace equation, there is also a non-trivial solution for Eq. (3) when the scale reaches a critical value. The implication of a degenerate scale in plane elasticity is same as in the case of Laplace equation. For example, the influence matrix of the weakly singular kernel (the logarithmic kernel $U^*_{ij}(\xi,x)$) might be singular. Alternatively speaking, the problem also originates from rank deficiency in the influence matrices. Numerical technique for evaluating the degenerate scale was also suggested by using two sets of some particular solution in the geometry of normal scale [10]. For the elliptic notch case, a closed form solution has been obtained by using the complex variable and elliptic coordinate [11]. It is proved that there are either two single critical values or one double critical value for any domain boundary. For two circle holes in an infinite plate, degenerate scales are also studied [12].

The degenerate scale problem for an ellipse-shaped region in BIE was studied [13]. Since there is no condition at remote place, the usual suggested kernel $U^{*2}_{ij}(\xi,x)$ (see Eq. (37)) can be used in the study. However, in the present study, there is a regularity condition at infinity for the exterior boundary value problem. Therefore, one must use the kernel $U^{*1}_{ij}(\xi,x)$ (see Eq. (34)) in the formulation of the degenerate scale problem for exterior boundary value problem.

Clearly, except for some simple cases, the degenerate scale problem for arbitrary configuration of notches cannot be solved in a closed form. Therefore, the degenerate scale problem in general case must be solved by using a numerical technique.

In this paper, a numerical technique for evaluating the degenerate scale in BIE is suggested. In the technique, the scale of a notch is changed gradually. Once the determinant for the influence matrix is nearly equal to zero, the degenerate scale is obtained. In addition, the eigenfunctions, or the non-trivial solutions, can also be evaluated. From the cases of elliptic and triangle notches, computed result proves that there are two critical values.

In addition, three numerical examples with the known exact solution are presented to examine the results obtained from numerical solution. In the examination, the suggested kernel $U^{*1}_{ij}(\xi,x)$ is used. In this case, we found that if the used size is near the critical value, the improper solution exists. However, if the used size is different from the critical value by 10%, the obtained numerical solution has a sufficient accuracy.

2. New BIE for exterior problem in plane elasticity with the usage of a suggested kernel $U^{*1}_{ij}(\xi,x)$

A new BIE for exterior problem in plane elasticity is introduced, in which the adopted kernel $U^{*1}_{ij}(\xi,x)$ (see Eq. (34)) is different by a constant from the usual one. It is proved that the regularity condition at infinity is satisfied by the usage of the suggested kernel when non-equilibrated loadings are applied on the contour. The role of regularity condition in BIE was introduced previously in Ref. [3].

2.1. Preliminary knowledge

The following analysis depends on the complex variable function method in plane elasticity [14]. In the method, the stresses $(\sigma_x,\sigma_y,\sigma_{xy})$, the resultant forces (X,Y) and the displacements (u,v) are expressed in terms of two complex potentials $\phi(z)$ and $\psi(z)$ such that

$$\sigma_x+\sigma_y=4\,\mathrm{Re}\,\phi'(z),$$

$$\sigma_y-\sigma_x+2\mathrm{i}\sigma_{xy}=2[\bar{z}\phi''(z)+\psi'(z)], \tag{4}$$

$$f=-Y+\mathrm{i}X=\phi(z)+z\overline{\phi'(z)}+\overline{\psi(z)}, \tag{5}$$

$$2G(u+\mathrm{i}v)=\kappa\phi(z)-z\overline{\phi'(z)}-\overline{\psi(z)}, \tag{6}$$

where $z=x$+iy denotes complex variable, G is the shear modulus of elasticity, $\kappa=(3-\nu)/(1+\nu)$ is for the plane stress problems, $\kappa=3-4\nu$ is for the plane strain problems, and ν is the Poisson's ratio. In the present study, the plane strain condition is assumed thoroughly. In the following, we occasionally rewrite the displacements "u", "v" as u_1, u_2, σ_x, σ_y, σ_{xy} as σ_{11}, σ_{22}, σ_{12}, and "x", "y" as x_1, x_2, respectively.

The first studied problem is about the representation form of a displacement–stress field. Two kinds of representation form are introduced below.

The first kind of form is called the pure deformable form. The following is an example. It is assumed that the complex potentials take the form:

$$\phi(z)=\ln z, \quad \psi(z)=-\kappa\ln z. \tag{7}$$

From Eq. (7), the stresses and displacements at a point $z=R\exp(\mathrm{i}\theta)$ are found as follows:

$$\sigma_x+\sigma_y=\frac{4\cos\theta}{R}, \quad \sigma_y-\sigma_x+2\mathrm{i}\sigma_{xy}=-\frac{2}{R}[\exp(-3\mathrm{i}\theta)+\kappa\exp(-\mathrm{i}\theta)],$$

$$2Gu=2\kappa\ln R-\cos 2\theta, \quad 2Gv=-\sin 2\theta. \tag{8}$$

Since the two pairs of the complex potentials, $\phi(z)=\ln z$, $\psi(z)=0$ and $\phi(z)=0$, $\psi(z)=-\kappa\ln z$ can cause non-vanishing displacements and stresses anywhere, therefore, the mentioned form belongs to the pure deformable form.

The second kind of form is called the impure deformable form. The following is an example. It is assumed that the complex potentials take the form

$$\phi(z)=\ln z, \quad \psi(z)=-\kappa\ln z+1. \tag{9}$$

From Eq. (9), the stresses and displacements at a point $z=R\exp(\mathrm{i}\theta)$ are found as follows:

$$\sigma_x+\sigma_y=\frac{4\cos\theta}{R}, \quad \sigma_y-\sigma_x+2\mathrm{i}\sigma_{xy}=-\frac{2}{R}[\exp(-3\mathrm{i}\theta)+\kappa\exp(-\mathrm{i}\theta)],$$

$$2Gu=2\kappa\ln R-2\cos^2\theta, \quad 2Gv=-\sin 2\theta. \tag{10}$$

Since the one pair of the complex potentials, or the pair $\phi(z)=0,\ \psi(z)=1$, only cause non-vanishing displacements ($2Gu=-1$ and $2Gv=0$), and the relevant stresses are equal to zero (or $\sigma_y=\sigma_x=\sigma_{xy}=0$) anywhere, therefore, the mentioned form shown by Eq. (10) belongs to the impure deformable form.

It is pointed out here that, it is difficult to find the impure deformable form from a displacement expression in the real variable. In fact, the displacements in Eq. (8) or (10) are expressed in the form of function of R and θ. In Eq. (8), the displacements take the expression $2Gu=2\kappa\ln R-\cos 2\theta,\quad 2Gv=-\sin 2\theta$. In addition, in Eq. (10) the displacements take the expression $2Gu=2\kappa\ln R-2\cos^2\theta,\quad 2Gv=-\sin 2\theta$. Clearly, both two sets of displacements represent an elasticity solution. However, it is difficult to find whether the displacements shown by Eq. (8) or (10) is expressed in the pure deformable form or not. However, it is straightforward to find the impure deformable form from the complex potentials, for example, from Eq. (9).

It is known that there are three pairs of complex potentials, which are related to rigid motions of body. Those pairs are as follows [14]:

$$\phi(z)=a_0,\quad \psi(z)=0, \tag{11}$$

$$\phi(z)=0,\quad \psi(z)=b_0, \tag{12}$$

$$\phi(z)=\mathrm{i}\gamma z,\quad \psi(z)=0\quad(\gamma-\text{real}). \tag{13}$$

Naturally, if some complex potentials possess the components shown by Eqs. (11), (12) or (13), the relevant displacement–stress fields must belong to the impure deformable form.

It is necessary to study the presentation form of displacement–stress field in the present analysis. The analysis has a close relation with the regularity condition at infinity and the formulation of integral equation for the exterior problem.

An important problem in the paper is to study the behavior of the MWDI (mutual work difference integral on the large circle) from two stress fields (the α-field and the β-field) [15,16]. The mentioned MWDI, or $D_{(\mathrm{CR})}$, is defined as follows:

$$D_{(\mathrm{CR})}=\oint_{(\mathrm{CR})}(u_{i(\alpha)}\sigma_{ij(\beta)}-u_{i(\beta)}\sigma_{ij(\alpha)})n_j\,\mathrm{d}s, \tag{14}$$

where the subscript CR denotes a sufficient large circle for integration, $u_{i(\alpha)},\sigma_{ij(\alpha)}(u_{i(\beta)},\sigma_{ij(\beta)})$ denotes the displacements and stresses in the α-field (the β-field), respectively, n_j is the direction cosines. The result for this integral has been obtained previously [16].

In the case of remote tractions being zero, a physical stress field with the name of α-field is introduced, which is defined by two complex potentials [14]:

$$\phi_{(\alpha)}(z)=A_2\ln z+a_0+\sum_{k=1}^{\infty}\frac{a_k}{z^k},$$
$$\psi_{(\alpha)}(z)=B_2\ln z+b_0+\sum_{k=1}^{\infty}\frac{b_k}{z^k}, \tag{15}$$

where

$$B_2=-\kappa\bar{A}_2,\quad A_2=-\frac{P_x+\mathrm{i}P_y}{2\pi(\kappa+1)} \tag{16}$$

and $P_x+\mathrm{i}P_y$ denotes the resultant force applied in the finite portion of infinite plate. For some particular situation mentioned below, the α-field has been written in the impure deformable form. This can be seen from the fact that two pairs of complex potentials, the pair $\phi(z)=a_0,\psi(z)=0$, and the pair $\phi(z)=0,\psi(z)=b_0$ are involved in Eq. (15)

Secondly, another physical stress field with the name of β-field is introduced, which is defined by

$$\phi_{(\beta)}(z)=E_2\ln z+\sum_{k=1}^{\infty}\frac{\mathrm{e}_k}{z^k},\quad \psi_{(\beta)}(z)=F_2\ln z+\sum_{k=1}^{\infty}\frac{f_k}{z^k}$$
$$(\text{with } F_2=-\kappa\bar{E}_2). \tag{17}$$

Note that, the β-field represents the physical field in the following analysis, and it now has been expressed in the pure deformable form, or no constant terms being involved in $\phi_{(\beta)}(z)$ and $\psi_{(\beta)}(z)$. Alternative speaking, each pair in Eq. (17) (for example, $\phi_{(\beta)}(z)=E_2\ln z,\ \psi_{(\beta)}(z)=0$) represents non-vanishing displacements and stresses anywhere.

After some manipulation, the following result for a path independent integral was obtained [16]

$$D_{(\mathrm{CR})}=\oint_{(\mathrm{CR})}(u_{i(\alpha)}\sigma_{ij(\beta)}-u_{i(\beta)}\sigma_{ij(\alpha)})n_j\,\mathrm{d}s$$
$$=-\frac{\pi(\kappa+1)}{G}\mathrm{Re}[a_0F_2+b_0E_2], \tag{18}$$

where "CR" is a sufficient large circle. It is valuable to describe the physical meaning of Eq. (18). In fact, the right-hand term of Eq. (18) represents a contribution to the MWDI from the terms a_0, b_0 (representing a rigid translation in the α-field) and the terms F_2, E_2 (representing resultant force in the β-field) has a contribution to the MWDI.

In the following, the α-field is related to the fundamental field caused by concentrated force at the point $z=t$ (Fig. 1). The relevant complex potentials are as follows [14]:

$$\phi(z)=F\ln(z-t),\quad \psi(z)=-\kappa\bar{F}\ln(z-t)-\frac{F\bar{t}}{z-t}, \tag{19}$$

where

$$F=-\frac{P_x+\mathrm{i}P_y}{2\pi(\kappa+1)}, \tag{20}$$

where $P_x+\mathrm{i}P_y$ is the concentrated force applied at the point $z=t$. Note that, the complex potentials shown by Eq. (19) is expressed in a pure deformable form. From the complex potentials shown by Eq. (19), a simple derivation will lead to the kernel $U_{ij}^{*1}(\xi,x)$ used later.

Alternatively, the α-field can be also expressed in a different form:

$$\phi(z)=F\ln(z-t),\quad \psi(z)=-\kappa\bar{F}\ln(z-t)-\frac{F\bar{t}}{z-t}+\bar{F}. \tag{21}$$

Note that, complex potentials shown by Eq. (21) are expressed in an impure deformable form. In fact, the pair $\phi(z)=0,\ \psi(z)=\bar{F}$ corresponds to $u=\text{const}$, $v=\text{const}$, and $\sigma_x=\sigma_y=\sigma_{xy}=0$. From the complex potentials shown by Eq. (21), a simple derivation will lead to the kernel $U_{ij}^{*2}(\xi,x)$ used later.

There are three particular cases studied below. In the first case, the α-field is expressed in a pure deformable form shown by Eq. (19) with the relevant kernel $U_{ij}^{*1}(\xi,x)$. The expression shown by Eq. (19) is equivalent to $a_0=b_0=0$ in Eq. (15). In addition, in the β-field some resultant forces are applied in the finite portion (Fig. 1). Therefore, substituting $a_0=b_0=0$ into Eq. (18) yields

$$D_{(\mathrm{CR})}=-\frac{\pi(\kappa+1)}{G}\mathrm{Re}[a_0F_2+b_0E_2]=0$$
$$(\text{because of } a_0=b_0=0). \tag{22}$$

It is seen from Eq. (22) that, if the complex potentials shown by Eq. (19) with the relevant kernel $U_{ij}^{*1}(\xi,x)$ are used, the term $D_{(\mathrm{CR})}$ vanishes, or $D_{(\mathrm{CR})}=0$.

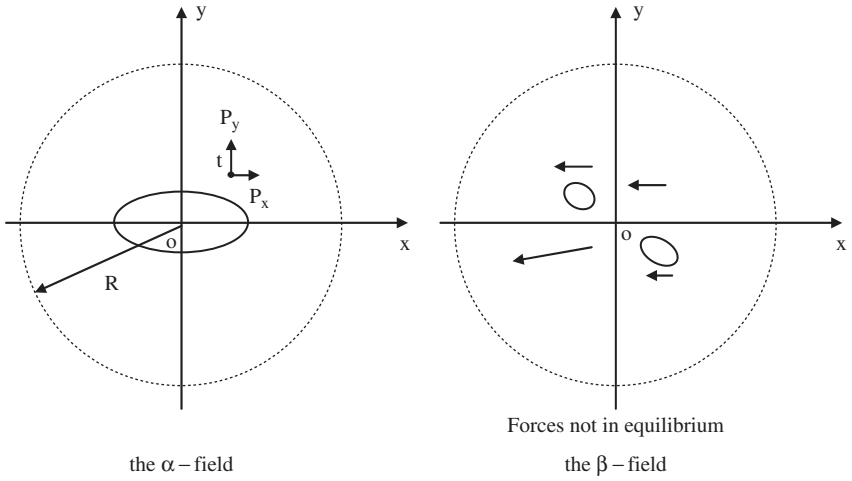

Fig. 1. (a) A concentrated force applied at the point $z = t$, or the loading condition for the α-field; (b) some loadings having resultant forces applied on a finite portion, or the loading condition for the β-field.

In the second case, the α-field is expressed in an impure deformable form shown by Eq. (21) with the relevant kernel $U_{ij}^{*2}(\xi, x)$. The complex potentials shown by Eq. (21) is equivalent to $a_0 = 0$ and $b_0 = \bar{F}$ in Eq. (15). In addition, some resultant forces are applied in the finite portion in the β-field (same as in the first case). Therefore, substituting $a_0 = 0$ and $b_0 = \bar{F}$ into Eq. (18) yields

$$D_{(\mathrm{CR})} = -\frac{\pi(\kappa+1)}{G}\mathrm{Re}[\bar{F}E_2] \neq 0. \tag{23}$$

It is seen from Eq. (23) that, if the complex potentials shown by Eq. (21) with the relevant kernel $U_{ij}^{*2}(\xi, x)$ are used, the term $D_{(\mathrm{CR})}$ does not vanish, or $D_{(\mathrm{CR})} \neq 0$.

In the third case, the α-field is expressed in a pure deformable form shown by Eq. (19) with the relevant kernel $U_{ij}^{*1}(\xi, x)$, or in an impure deformable form shown by Eq. (21) with the relevant kernel $U_{ij}^{*2}(\xi, x)$. In addition, in the β-field the applied forces on the finite region are in equilibrium (Fig. 2). In this case, we have $E_2 = F_2 = 0$ in Eq. (17). Under this combination for the α-field and the β-field, we will find

$$D_{(\mathrm{CR})} = -\frac{\pi(\kappa+1)}{G}\mathrm{Re}[a_0F_2 + b_0E_2] = 0 \quad (\text{because of } F_2 = E_2 = 0). \tag{24}$$

It is seen from Eq. (24) that, if the applied forces on the finite region of the β-field are in equilibrium, then $D_{(\mathrm{CR})} = 0$ without regarding the usage of the complex potentials shown by Eq. (19) or (21) with relevant kernels $U_{ij}^{*1}(\xi, x)$ or $U_{ij}^{*2}(\xi, x)$. On the other hand, from the following estimation $u_{i(\alpha)} = O(\ln(R))$, $\sigma_{ij(\alpha)} = O(1/R)$, $u_{i(\beta)} = O(1/R)$, $\sigma_{ij(\beta)} = O(1/R^2)$, we have

$$\begin{aligned} D_{(\mathrm{CR})} &= \oint_{(\mathrm{CR})} (u_{i(\alpha)}\sigma_{ij(\beta)} - u_{i(\beta)}\sigma_{ij(\alpha)})n_j \,\mathrm{d}s \\ &= \lim_{R\to\infty} \int_0^{2\pi} \left\{ O\ln(R)O\left(\frac{1}{R^2}\right) - O\left(\frac{1}{R}\right)O\left(\frac{1}{R}\right)\right\} R\,\mathrm{d}\theta \\ &= 0. \end{aligned} \tag{25}$$

Therefore, the result shown by Eq. (24) is easy to see. In fact, Eq. (25) was indicted in Ref. [3].

In order to make a comparison among three cases, a summary for properties of three cases is presented in Table 1.

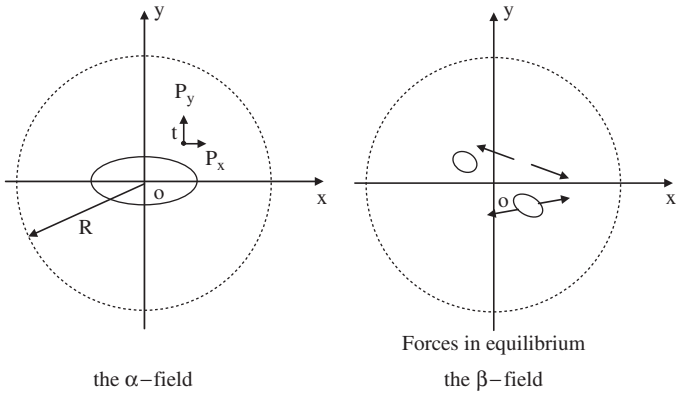

Fig. 2. (a) A concentrated force applied at the point $z = t$, or the loading condition for the α-field; (b) some loadings in equilibrium applied on a finite portion, or the loading condition for the β-field.

Table 1
Properties of $D_{(\mathrm{CR})}$ for different representation forms for the α-field, and different loading conditions for β-field

	The α-field, for the fundamental solution	The β-field, for the physical field	Result
Case 1	Displacements expressed in pure deformable form with the usage of $U_{ij}^{*1}(\xi, x)$	With a non-equilibrated loadings on the contour	$D_{(\mathrm{CR})} = 0$
Case 2	Displacements expressed in impure deformable form with the usage of $U_{ij}^{*2}(\xi, x)$	With a non-equilibrated loadings on the contour	$D_{(\mathrm{CR})} \neq 0$
Case 3	Displacements expressed in pure deformable form with the usage of $U_{ij}^{*1}(\xi, x)$ or in impure deformable form with the usage of $U_{ij}^{2}(\xi, x)$	With an equilibrated loadings on the contour	$D_{(\mathrm{CR})} = 0$

2.2. Formulation of new suggested BIE for exterior region in an infinite plate

Without losing generality, we can introduce the BIE for the region between the elliptic contour Γ and a large circle "CR"

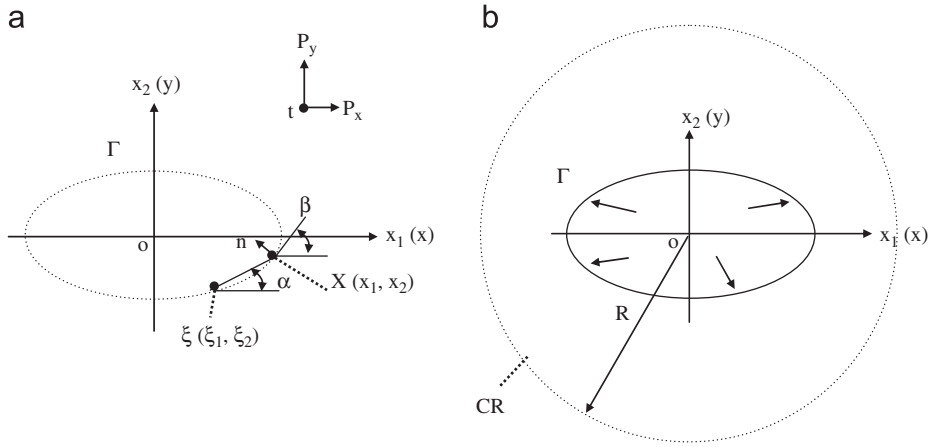

Fig. 3. (a) A concentrated force applied at the point $z = t$, or the loading condition for the α-field; (b) some loadings having resultant forces applied on the elliptic contour, or the loading condition for the β-field.

(Fig. 3). The observation point ξ is assumed on the elliptic contour $\xi \in \Gamma$. For the plane strain case, the suggested BIE can be written as follows:

$$\frac{1}{2}u_i(\xi) + \int_\Gamma P^*_{ij}(\xi,x)u_j(x)\,ds(x) = \int_\Gamma U^{*1}_{ij}(\xi,x)p_j(x)\,ds(x) + D^{*1}_{i(CR)}(\xi), \quad (i = 1,2, \xi \in \Gamma), \tag{26}$$

where $D^{*1}_{i(CR)}(\xi)$ in a mutual work difference integral (abbreviated as MWDI) on a large circle and is defined by

$$D^{*1}_{i(CR)}(\xi) = -\int_{CR} P^*_{ij}(\xi,x)u_j(x)\,ds(x) + \int_{CR} U^{*1}_{ij}(\xi,x)p_j(x)\,ds(x) \tag{27}$$

and the kernel $P^*_{ij}(\xi,x)$ is defined by [3]

$$P^*_{ij}(\xi,x) = -\frac{1}{4\pi(1-\nu)}\frac{1}{r}\{(r_{,1}n_1 + r_{,2}n_2)((1-2\nu) \times \delta_{ij} + 2r_{,i}r_{,j}) + (1-2\nu)(n_i r_{,j} - n_j r_{,i})\}, \tag{28}$$

where Kronecker deltas δ_{ij} is defined as, $\delta_{ij} = 1$ for $i = j$, $\delta_{ij} = 0$ for $i \neq j$, and

$$r_{,1} = \frac{x_1 - \xi_1}{r} = \cos\alpha, \quad r_{,2} = \frac{x_2 - \xi_2}{r} = \sin\alpha,$$

$$n_1 = -\sin\beta, \quad n_2 = \cos\beta, \tag{29}$$

where the angles α and β are indicated in Fig. 3(a).

The kernel $P^*_{ij}(\xi,x)$ can be obtained in a usual way [3]. The kernel $U^{*1}_{ij}(\xi,x)$ may be obtained from the fundamental stress field (Fig. 3(a)), and the relevant complex potentials have been shown in Eq. (19).

Making use of Eqs. (6) and (19) yields

$$2G(u + \mathrm{i}v) = 2\kappa F \ln(r) - \bar{F}\frac{z-t}{\bar{z}-\bar{t}}, \quad \text{where } r = |z-t|. \tag{30}$$

In the derivation, let the point "t" approach to the boundary point ξ of ellipse, and the point "z" to the boundary point "X" (Fig. 3(a)), and

$$z - t = r\exp(\mathrm{i}\alpha). \tag{31}$$

If letting $P_x = 1$ and $P_y = 0$, from Eqs. (20) and (30) we have

$$u = \frac{1}{8\pi(1-\nu)G}\{-(3-4\nu)\ln(r)\delta_{ij} + \cos^2\alpha - 0.5\},$$
$$v = \frac{1}{8\pi(1-\nu)G}\{\sin\alpha\cos\alpha\}. \tag{32}$$

If letting $P_x = 0$ and $P_y = 1$, from Eqs. (20) and (30) we have

$$u = \frac{1}{8\pi(1-\nu)G}\{\sin\alpha\cos\alpha\},$$
$$v = \frac{1}{8\pi(1-\nu)G}\{-(3-4\nu)\ln(r)\delta_{ij} + \sin^2\alpha - 0.5\}. \tag{33}$$

The mentioned derivation leads to

$$U^{*1}_{ij}(\xi,x) = \frac{1}{8\pi(1-\nu)G}\{-(3-4\nu)\ln(r)\delta_{ij} + r_{,i}r_{,j} - 0.5\delta_{ij}\}. \tag{34}$$

In the present case, the complex potentials for the α-field shown by Eq. (19) are expressed in the pure deformable form, which is used for deriving the kernel $U^{*1}_{ij}(\xi,x)$. Therefore, directly using Eq. (22) yields

$$D^{*1}_{i(CR)}(\xi) = 0 \quad (i = 1,2). \tag{35}$$

Therefore, from Eq. (26), the BIE is modified to be

$$\frac{1}{2}u_i(\xi) + \int_\Gamma P^*_{ij}(\xi,x)u_j(x)\,ds(x) = \int_\Gamma U^{*1}_{ij}(\xi,x)p_j(x)\,ds(x), \quad (i = 1,2, \quad \xi \in \Gamma) \quad (\xi \in \Gamma) \tag{36}$$

Similarly, from the complex potentials shown by Eq. (21), the following kernel is obtained:

$$U^{*2}_{ij}(\xi,x) = \frac{1}{8\pi(1-\nu)G}\{-(3-4\nu)\ln(r)\delta_{ij} + r_{,i}r_{,j}\}. \tag{37}$$

For the plane strain case, the BIE can be written as follows:

$$\frac{1}{2}u_i(\xi) + \int_\Gamma P^*_{ij}(\xi,x)u_j(x)\,ds(x) = \int_\Gamma U^{*2}_{ij}(\xi,x)p_j(x)\,ds(x) + D^{*2}_{i(CR)}(\xi), \quad (i = 1,2, \quad \xi \in \Gamma), \tag{38}$$

where $D^{*2}_{i(CR)}(\xi)$ in a mutual work difference integral (abbreviated as MWDI) on a large circle and is defined by

$$D^{*2}_{i(CR)}(\xi) = -\int_{CR} P^*_{ij}(\xi,x)u_j(x)\,ds(x) + \int_{CR} U^{*2}_{ij}(\xi,x)p_j(x)\,ds(x). \tag{39}$$

There are two cases under consideration. In the first case, the loading applied on the finite portion in the β-field is not in

equilibrium. In this case, from Eq. (23) we have $D^{*2}_{i(CR)}(\xi)\neq 0$, and the term $D^{*2}_{i(CR)}(\xi)$ in Eq. (38) cannot be dropped.

In the second case, the loading applied on the finite portion in the β-field is in equilibrium. In this case, from Eq. (24) we have $D^{*2}_{i(CR)}(\xi)=0$, and the term $D^{*2}_{i(CR)}(\xi)$ in Eq. (38) can be dropped. Therefore, substituting $D^{*2}_{i(CR)}(\xi)=0$ into Eq. (38) yields

$$\frac{1}{2}u_i(\xi)+\int_\Gamma P^*_{ij}(\xi,x)u_j(x)\,ds(x) = \int_\Gamma U^{*2}_{ij}(\xi,x)p_j(x)\,ds(x) \quad (i=1,2,\quad \xi\in\Gamma). \tag{40}$$

From above derivation we see that the BIE shown by Eq. (40) can only be used to the case that the loadings applied on the contour are in equilibrium, and it cannot be used to the case of non-equilibrated loadings on the contour.

It is seen that the BIE shown by Eq. (36) with the usage $U^{*1}_{ij}(\xi,x)$ can be used to arbitrary loading case. In addition, for the case of the loadings $p_j(x)$ in equilibrium, the results from the usage of the kernel $U^{*1}_{ij}(\xi,x)$ or $U^{*2}_{ij}(\xi,x)$ are equivalent. In fact, from Eq. (34) and (37), the following result is obtainable

$$\int_\Gamma (U^{*1}_{ij}(\xi,x)-U^{*2}_{ij}(\xi,x))p_j(x)\,ds(x) = -\frac{1}{16\pi(1-\nu)G} \times\int_\Gamma \delta_{ij}p_j(x)\,ds(x)=0. \tag{41}$$

Therefore, the mentioned statement is proved.

It is seen that, any boundary values for the displacements and stresses from a pure deformable form in the exterior problem must satisfy the BIE shown by Eq. (36). Actually, we have performed the following examination. In the numerical examination, the complex potentials take the form $\phi(z)=F\ln z$, $\psi(z)=-F\ln z$ (F-real). Further, one substitutes the relevant displacements along the boundary in the left-hand side of Eq. (36), and substitutes the relevant stresses in the right-hand side of Eq. (36), then, the validity of Eq. (36) has been found.

People may meet the following situation. If one substitutes an elasticity solution, for example, $u=1$, $v=0$ and $\sigma_x=\sigma_y=\sigma_{xy}=0$ into Eq. (36), the equality shown by Eq. (36) is not valid. The reason for the happened discrepancy can be expressed as follows. In fact, all the derivations for the BIE shown by Eq. (36) are based on the fact that both the α-field and β-field are expressed in the pure deformable form. Alternative speaking, one do not allow any solutions in the impure deformable form or in the rigid motion form (for example, $u=1$, $v=0$ for displacement and $\sigma_x=\sigma_y=\sigma_{xy}=0$ for stresses) to verify the BIE shown by Eq. (36).

2.3. Examination for the usage of the suggested kernel $U^{*1}_{ij}(\xi,x)$

One possibility for examination of the correctness for the usage of the kernel $U^{*1}_{ij}(\xi,x)$ is from solution of degenerate scale problem. For the circle hole case ($a=b$), by using the elliptic coordinates and complex variable, the closed form solution was found [11]

$$a=1. \tag{42}$$

On the other hand, from Eq. (36) we can propose the following humongous equation

$$\int_\Gamma U^{*1}_{ij}(\xi,x)p_j(x)\,ds(x)=0 \quad (i=1,2,\quad \xi\in\Gamma). \tag{43}$$

For circle hole case, a closed form solution for Eq. (43) suggested later also indicates that the degenerate scale is $a=1$. In addition, a numerical solution for Eq. (43) (see below, next paragraph and Table 2) indicates that the degenerate scale is $a=1.00026$.

In the same time, the following integral equation with the usage of $U^{*2}_{ij}(\xi,x)$ is introduced [8,9]

$$\int_\Gamma U^{*2}_{ij}(\xi,x)p_j(x)\,ds(x)=0 \quad (i=1,2,\quad \xi\in\Gamma) \quad (\xi\in\Gamma). \tag{44}$$

The degenerate scale for the circular hole is $a=\exp(1/2\kappa)$ ($=1.32019$, for $\nu=0.3$ and plane strain case). This mentioned result reveals that the usage of kernel $U^{*2}_{ij}(\xi,x)$ is also not reasonable in the degenerate scale problem.

3. Degenerate scale problem

The degenerate scale problem is a particular problem in BIE. In the formulation, we take the elliptic notch in an infinite plate as example (Fig. 4(a)). Assume that the major half-axis "a" is a parameter subject to change, and the ratio b/a is given beforehand. It is preferable to write the kernel $U^{*1}_{ij}(\xi,x)$ in the form of $U^{*1}_{ij}(\xi,x,a)$. Substituting $u_j=0$ ($j=1,2$) in the left side of Eq. (36) yields

$$\int_\Gamma U^{*1}_{ij}(\xi,x,a)p_j(x)\,ds(x)=0 \quad (i=1,2,\quad \xi\in\Gamma). \tag{45}$$

In addition, it is preferable to write Eq. (45) in the form

$$J_i=0,\quad \text{where } J_i=\int_\Gamma U^{*1}_{ij}(\xi,x,a)p_j(x)\,ds(x) \quad (i=1,2,\quad \xi\in\Gamma). \tag{46}$$

In the degenerate scale problem, we will find a particular value of "a" such that Eq. (45) or (46) has a non-trivial solution. Here, $p_j=0$ ($j=1,2$) is a trivial solution for Eq. (45) or (46).

A closed form solution for the circle hole case ($b/a=1$) is introduced below [8]. If substituting $p_1=g_0$ and $p_2=0$ (for $x(x_1,x_2)\in\Gamma$) in Eq. (46), after some manipulations we obtain

$$J_1=H\pi a g_0[2(3-4\nu)\ln a],\quad \text{where } H=\frac{-1}{8\pi(1-\nu)G} \quad (\text{for } \xi\in\Gamma),$$

$$J_2=0 \quad (\text{for } \xi\in\Gamma). \tag{47}$$

From Eq. (47), it is suitable to find a solution for "a" from

$$\ln a=0. \tag{48}$$

Table 2
Two critical values for the elliptic notch: (1) $a=\lambda_1=f_1(b/a)$ and $a=\lambda_2=f_2(b/a)$ in the case of using the kernel $U^{*1}_{ij}(\xi,x,a)$ (see Eq. (34)), (2) $a=\lambda_1=g_1(b/a)$ and $a=\lambda_2=g_2(b/a)$ in the case of using the kernel $U^{*2}_{ij}(\xi,x,a)$ (see Eq. (37)), within the range $0.1\leqslant b/a\leqslant 1.0$ (see Fig. 4(a))

b/a	0.1	0.2	0.3	0.4	0.5	0.6	0.7	0.8	0.9	1.0
f_1	2.28277	2.00630	1.78718	1.60963	1.46310	1.34027	1.23592	1.14626	1.06843	1.00028
f_{1^*}	2.28213	2.00574	1.78667	1.60918	1.46269	1.33989	1.23558	1.14594	1.06813	1.00000
f_2	1.44896	1.38531	1.32510	1.26859	1.21576	1.16647	1.12050	1.07764	1.03764	1.00028
f_{2^*}	1.44855	1.38492	1.32473	1.26824	1.21542	1.16614	1.12019	1.07734	1.03735	1.00000
g_1	3.01370	2.64871	2.35942	2.12502	1.93157	1.76941	1.63166	1.51329	1.41054	1.32056
g_2	1.91290	1.82887	1.74939	1.67479	1.60504	1.53996	1.47928	1.42270	1.36989	1.32056

f_{1^*}, f_{2^*} from a closed form solution [11].

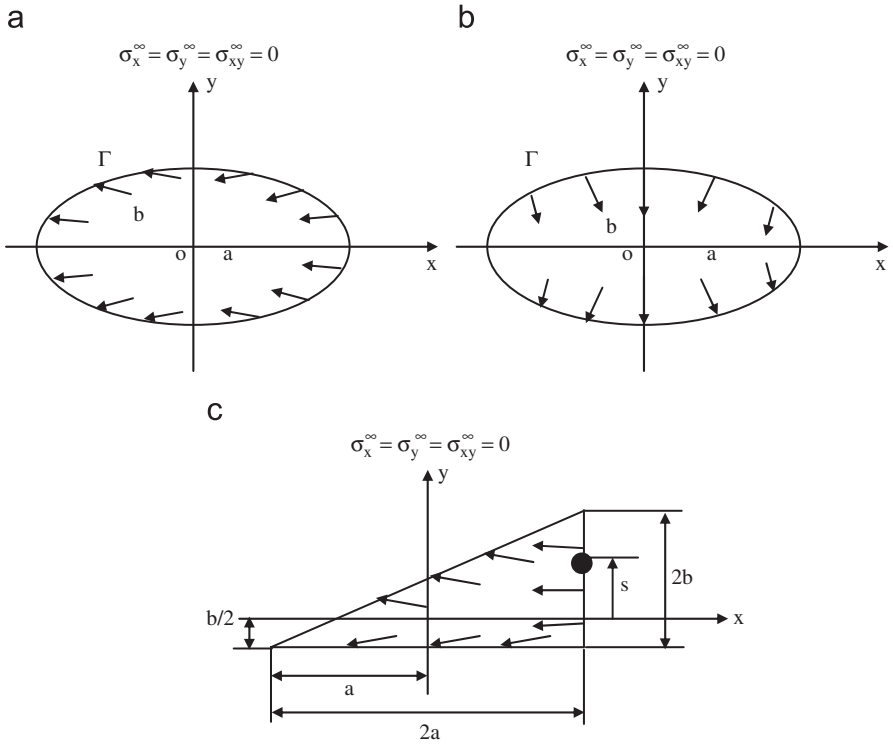

Fig. 4. Three cases of configuration: (a) an elliptic notch with loadings having a resultant force in *x*-direction; (b) an elliptic notch with loadings having a resultant force in *y*-direction; (c) a triangle notch with loadings having a resultant force in *x*-direction.

Therefore, the solution for Eq. (48) can be found

$$a = \lambda, \quad \text{where } \lambda = \exp[0] = 1. \tag{49}$$

The obtained value for $a = \lambda = 1$ is called the critical value for size hereafter.

From above-mentioned analysis, the following conclusion is deduced. If the critical $a = \lambda = 1$ is adopted, $p_1 = g_0$ (g_0, any constant value), $p_2 = 0$ (for $x(x_1, x_2) \in \Gamma$) is a non-trivial solution for the integral Eq. (45) in the case of a circular hole.

It is seen that from the Dirichlet problem of interior domain, the relevant homogenous equation takes the same form as shown by Eq. (45). Therefore, the degenerate scale problems arising from exterior region and interior domain are the same.

For the ellipse contour, a closed form solution for the critical value was obtained with the usage of the complex variable and the elliptic coordinate [11]. In addition, the critical value can also be evaluated by some particular solutions on the normal scale. The relevant derivation for the Laplace equation and for the plane elasticity can be referred to in Refs. [5,10]. It is easy seen that it is more difficult to obtain the critical value in some complicated cases of contour configuration.

4. Numerical evaluation of the degenerate scale and numerical examination for the correctness of usage of the kernel $U_{ij}^*(\xi, x)$

In the paragraph, the following two problems are studied numerically. The first is about the degenerate scale for some shapes of contour. Because of inherent difficulties in integration, we cannot obtain the critical value for an arbitrary notch configuration in a closed form. Therefore, a numerical technique is suggested for the evaluation of the critical value. Discretization of the BIE is a necessary step in the numerical analysis. After discretization, the critical value and the non-trivial solution are obtained numerically.

The second problem is to prove the correctness of usage of the kernel $U_{ij}^{*1}(\xi, x)$. Assume that the degenerate scale is not reached. In this case, we choose an exact solution, for example, the solution defined by the complex potentials $\phi(z) = Q_0 \ln z$, $\psi(z) = -\kappa Q_0 \ln z$, which represent some non-equilibrated loadings on the contour. In this case, we formulate the Dirichlet problem for the exterior domain for some shapes of contour. The displacements $u_j(x)$ ($j = 1, 2$) from the closed form solution are substituted into the BIE shown by Eq. (36), and obtain the traction $p_j(x)$ ($j = 1, 2$) from the BIE. Further, the obtained numerical results for tractions $p_j(x)$ ($i = 1, 2$) are compared with those $p_j(x)$ ($i = 1, 2$) from the exact solution. This kind of computation can examine if the usage of the $U_{ij}^{*1}(\xi, x)$ is correct or not. The following examples actually prove that the correctness of the usage of the kernel $U_{ij}^{*1}(\xi, x)$.

4.1. Numerical evaluation of the critical value and non-trivial solution for homogenous equation

Without losing generality, the elliptic notch with two half-axes "*a*" and "*b*" in infinite plate is taken as an example (Fig. 4(a)). In the numerical technique, the ellipse is divided into 120 intervals, and $\nu = 0.3$ is assumed. The constant traction is assumed for each interval. After making discretization, Eq. (45) may be written in the following form:

$$\sum_{n=1}^{M} U_{mn} \tilde{p}_n = 0 \quad (m = 1, 2, \ldots, M), \tag{50}$$

where the matrix U_{mn} ($m, n = 1, \ldots, M$) is derived from the kernel function $U_{ij}^{*1}(\xi, x)$, and $\tilde{p}_n$ denotes the loading vector that is assumed on the nodes. The vector $\tilde{p}_n (i = 1, 2, \ldots)$ is composed of $p_{1(i)}, p_{2(i)}$ ($i = 1, 2, \ldots$). Eq. (50) may be written in a matrix form as follows:

$$\mathbf{U}\tilde{\mathbf{p}} = 0 \quad \text{or} \quad \mathbf{U}(\mathbf{a})\tilde{\mathbf{p}} = 0. \tag{51}$$

We assume that the ratio b/a is given beforehand. Therefore, the parameter, or the major half-axis "a" is only one parameter involved in the matrix $\mathbf{U}$. To distinguish this situation, the matrix $\mathbf{U}$ is rewritten as $\mathbf{U}(a)$.

The critical value "a" is evaluated from the following equation

$$\det(\mathbf{U}(\mathbf{a})) = 0. \tag{52}$$

In a real computation, the degenerate scale critical value "a" is evaluated by the following technique. A sufficient small value δ is assumed in advance (use $\delta = 1 \times 10^{-6}$ in this paper). Once we find a value for λ such that $\det(U)|_{a=\lambda-\delta} > 0$ and $\det(U)|_{a=\lambda+\delta} < 0$ (or $\det(U)|_{a=\lambda-\delta} < 0$ and $\det(U)|_{a=\lambda+\delta} > 0$), the critical value $a = \lambda$ is obtained approximately.

For the ratio b/a within the range $0.1 < b/a < 1$, two critical values $a = \lambda_1$ and $a = \lambda_2$ were found from the computation. In the case of using the kernel $U_{ij}^{*1}(\xi, x, a)$, the obtained critical values are expressed as

$$\lambda_1 = f_1\left(\frac{b}{a}\right), \quad \lambda_2 = f_2\left(\frac{b}{a}\right). \tag{53}$$

The computed results for $f_1(b/a)$, $f_2(b/a)$ are listed in Table 2. It can be seen from the tabulated results that, when $b/a = 1$, the two degenerate scale critical values are merged into one value $a = \lambda_1 = \lambda_2 = 1.00028$. Besides, the exact one takes the value $a = \lambda_1 = \lambda_2 = 1$.

By using complex variable and elliptic coordinate, the degenerate scales for elliptic contour were found in a closed form [11], which are as follows:

$$a = \lambda_1 = f_{1*}\left(\frac{b}{a}\right) = \frac{2}{1+\delta}\exp\left(\frac{1-\delta}{2\kappa(1+\delta)}\right),$$

$$a = \lambda_2 = f_{2*}\left(\frac{b}{a}\right) = \frac{2}{1+\delta}\exp\left(-\frac{1-\delta}{2\kappa(1+\delta)}\right) \quad \left(\text{with } \delta = \frac{b}{a}\right). \tag{54}$$

The obtained results for $f_{1*}(b/a)$ and $f_{2*}(b/a)$ are also listed in Table 2. From comparison results in Table 2 we see that there is no significant deviation between numerical result and exact solution.

The $b/a = 0.5$ case is taken as an example to find the non-trivial solution for $\tilde{p}_n$. As mentioned above, two critical values, $a = \lambda_1 = 1.46310$ and $a = \lambda_2 = 1.21576$ (for $b/a = 0.5$ case), have been achieved approximately. The non-trivial solution for $\tilde{p}_n$ can be found in the following manner. After taking $a = \lambda_1 = 1.46310$, we can formulate the matrix "$\mathbf{U}$" with the elements U_{mn} ($m, n = 1, \ldots, M$) as a first step. Substituting $\tilde{p}_1 = 1$ in Eq. (50) yields

$$\sum_{n=2}^{M} U_{mn}\tilde{p}_n = -U_{m1} \quad (m = 1, 2, \ldots, M). \tag{55}$$

We may truncate $M-1$ equations from Eq. (55), and obtain

$$\sum_{n=2}^{M} U_{mn}\tilde{p}_n = -U_{m1} \quad (m = 2, \ldots, M). \tag{56}$$

From Eq. (56), we can obtain a solution for $\tilde{p}_n (n = 2, 3, \ldots, M)$. In the case of assuming $f_x(\theta)|_{\theta=0^\circ} = 1$, two functions $f_x(\theta)$ and $f_y(\theta)$ can be obtained immediately. The computed results for tractions are expressed as follows:

$$p_1 = f_x(\theta), \quad p_2 = f_y(\theta)$$
(tractions at the boundary points, $x = a\cos\theta, \quad y = b\cos\theta$) (57)

Both functions $f_x(\theta), f_y(\theta)$ are plotted in Fig. 5. From computed results, it is found that $f_y(\theta) = 0.000$. That is to say, the critical value $a = \lambda_1 = 1.46310$ only gives the component p_1 the non-trivial solution. Similar phenomena can be found in the non-homogenous equation case (see Eq. (63)).

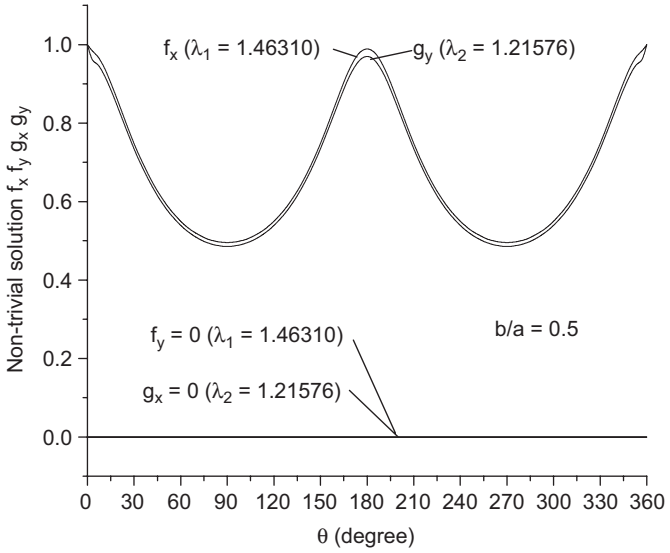

Fig. 5. Non-trivial solution for the boundary tractions on the elliptic notch ($b/a = 0.5$): (a) $f_x(\theta)$and $f_y(\theta) = 0$ in the case of $a = \lambda_1 = 1.46310$; (b) $g_x(\theta) = 0$ and $g_y(\theta)$ in the case of $a = \lambda_2 = 1.21576$ (see Fig. 4(a) and Eqs. (57) and (58)).

Similarly, for the second critical value $a = \lambda_2 = 1.21576$ (for $b/a = 0.5$ case), the non-trivial solution for $\tilde{p}_n$ can be found in a similar manner. The computed results for tractions under the condition $g_y(\theta)|_{\theta=0^\circ} = 1$ are expressed as follows:

$$p_1 = g_x(\theta), \quad p_2 = g_y(\theta)$$
(tractions at the boundary points, $x = a\cos\theta, \quad y = b\cos\theta$) (58)

Both functions $g_x(\theta), g_y(\theta)$ are also plotted in Fig. 5. It is found that the function $g_x(\theta)$ takes the value $g_x(\theta) = 0.000$. That is to say, the critical value $a = \lambda_2 = 1.21576$ only gives the component p_2 the non-trivial solution. Similar phenomena can be found in the non-homogenous equation case (see Eq. (63)).

The used kernel in the integral equation will influence the results about the critical value. Instead of the kernel $U_{ij}^{*1}(\xi, x, a)$, we may propose the following integral equation

$$\int_\Gamma U_{ij}^{*2}(\xi, x, a) p_j(x)\, \mathrm{d}s(x) = 0 \quad (i = 1, 2, \quad \xi \in \Gamma), \tag{59}$$

where

$$U_{ij}^{*2}(\xi, x) = \frac{1}{8\pi(1-\nu)G}\{-(3-4\nu)\ln(r)\delta_{ij} + r_{,i}r_{,j}\}. \tag{60}$$

The kernel $U_{ij}^{*2}(\xi, x)$ is different by a constant $-\delta_{ij}/16\pi(1-\nu)G$ with respect to $U_{ij}^{*1}(\xi, x)$. The kernel $U_{ij}^{*2}(\xi, x)$ was introduced in Ref. [3].

Similarly, in the case of using the kernel $U_{ij}^{*2}(\xi, x, a)$, the obtained critical values are expressed as

$$\lambda_1 = g_1\left(\frac{b}{a}\right), \quad \lambda_2 = g_2\left(\frac{b}{a}\right). \tag{61}$$

The computed results for $g_1(b/a)$, $g_2(b/a)$ are also listed in Table 2. It is seen that the $g_1(b/a)$ and $g_2(b/a)$ values are larger than $f_1(b/a)$ and $f_2(b/a)$, respectively. It can be seen from the tabulated results that, when $b/a = 1$, the two critical values are merged into one value $a = \lambda_1 = \lambda_2 = 1.32056$. Besides, the exact one takes the value $a = \lambda_1 = \lambda_2 = 1.32019$ for the case of $\nu = 0.3$.

4.2. Numerical examination for the non-homogenous equation

From Eq. (36), the BIE can be rewritten as

$$\int_\Gamma U_{ij}^{*1}(\xi,x)p_j(x)\,ds(x) = h_i(\xi) \quad (i=1,2,\quad \xi\in\Gamma)\quad (\xi\in\Gamma), \tag{62}$$

where

$$h_i(\xi) = \frac{1}{2}u_i(\xi) + \int_\Gamma P_{ij}^{*}(\xi,x)u_j(x)\,ds(x) \quad (i=1,2,\quad \xi\in\Gamma)\quad (\xi\in\Gamma). \tag{63}$$

In the solution, the functions $u_j(x)$ $(j=1,2)$ are given beforehand. In addition, the functions $h_i(\xi)$ $(i=1,2)$ are obtained from Eq. (63), and they become the right-hand term of Eq. (62). In the following computation, we will find some particular behaviors for the solution of Eq. (62) once the critical values are approaching.

Example 4.1. The above-mentioned results for the critical value can be examined by the following concrete example. In the example shown by Fig. 4(a), we propose the following complex potentials

$$\phi(z) = Q_0 \ln z, \quad \psi(z) = -\kappa Q_0 \ln z, \tag{64}$$

where Q_0 is a loading that has a dimension of force. Therefore, from Eqs. (4) and (5), the stresses and the displacements can be evaluated

$$\sigma_x+\sigma_y = 4Q_0\,\mathrm{Re}\,\frac{1}{z},$$
$$\sigma_y-\sigma_x+2i\sigma_{xy} = -2Q_0\left(\frac{\bar z}{z^2}+\frac{\kappa}{z}\right), \tag{65}$$

$$2G(u+iv) = Q_0\left(2\kappa\ln|z| - \frac{z}{\bar z}\right). \tag{66}$$

In addition, from Eqs. (5) and (64) the amount of the resultant force in x-direction applied on the boundary will be $2\pi(\kappa+1)Q_0$. The relevant loading condition is shown in Fig. 4(a) approximately.

In the numerical examination, the BIE takes the form of Eq. (62). The displacements $u_j(x)$ $(j=1,2)$ obtained from the exact solution are substituted into Eq. (63), and the obtained results become the right-hand side of Eq. (62), the boundary tractions $p_j(x)$ $(j=1,2)$ will be obtained from Eq. (62).

In computation, the exterior ellipse has the two half-axes "a" and "b" with the ratio $b/a=0.5$ (Fig. 4(a)). The contour of ellipse is divided into 120 intervals. The constant displacement and traction are assumed for each interval. Standard numerical technique is used to solve the BIE Eq. (62) numerically.

As mentioned previously, there are two critical values $a=\lambda_1=1.46310$ and $a=\lambda_2=1.21576$ (for $b/a=0.5$ case), which have been shown in Table 2.

In this example, computations for five cases, $a=\lambda_1-\varepsilon$, $a=\lambda_1$, $a=\lambda_1+\varepsilon$, $a=0.9\lambda_1$, and $a=1.1\lambda_1$ $(\lambda_1=1.46310,\ \varepsilon=0.00002)$ are performed. The computed results for tractions are expressed as follows:

$$p_1 = f_x(\theta)\frac{\pi(\kappa+1)Q_0}{a},\quad p_2 = f_y(\theta)\frac{\pi(\kappa+1)Q_0}{a}$$
(tractions at the boundary points,
$x=a\cos\theta,\quad y=b\cos\theta$). (67)

The computed results for $f_x(\theta)$, and $f_y(\theta)$ are plotted in Figs. 6–8. For comparison, the exact result from Eq. (65) is also shown in the figures.

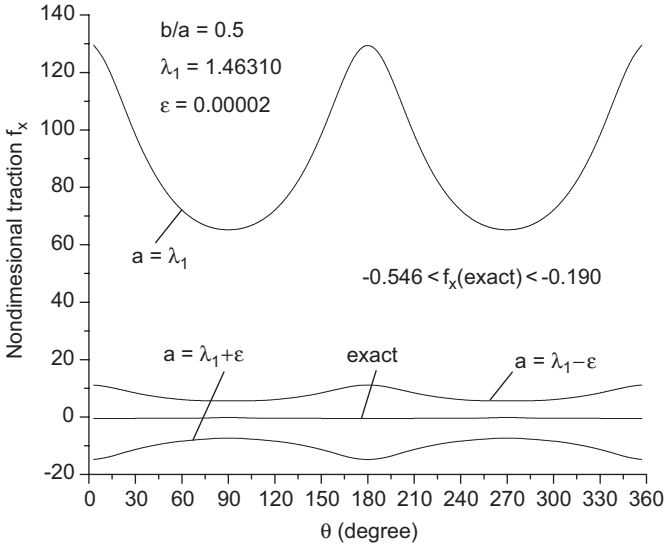

Fig. 6. Non-dimensional boundary tractions $f_x(\theta)$ on the elliptic boundary under the conditions: (a) $b/a=0.5$; (b) the assumed displacements from Eq. (64); (c) for three cases: $a=\lambda_1-\varepsilon$, $a=\lambda_1$ and $a=\lambda_1+\varepsilon$ $(\lambda_1=1.46310,\ \varepsilon=0.00002)$ (see Fig. 4(a) and Eq. (67)).

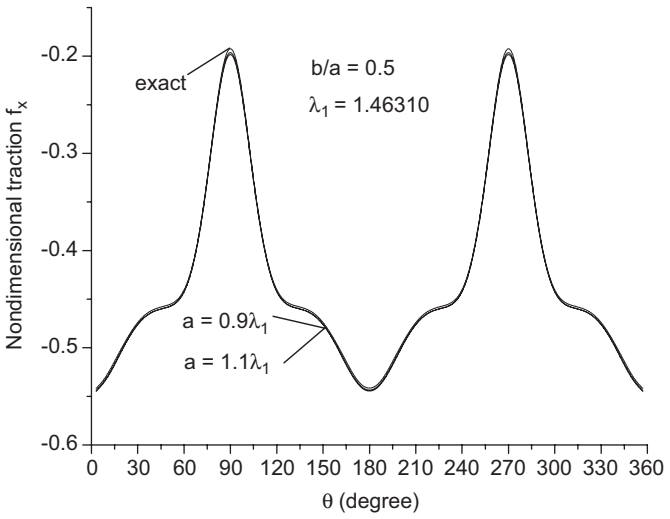

Fig. 7. Non-dimensional boundary tractions $f_x(\theta)$ on the elliptic boundary under the conditions: (a) $b/a=0.5$; (b) the assumed displacements from Eq. (64); (c) for two cases: $a=0.9\lambda_1$ and $a=1.1\lambda_1$ $(\lambda_1=1.46310)$ (see Fig. 4(a) and Eq. (67)).

The most significant feature of the critical value can be seen from Figs. 6 and 7. In fact, the exact values for $f_x(\theta)$ are varying within the range $-0.546\leqslant f_x(\theta)\leqslant -0.190$ (see Fig. 7). However, if $a=\lambda_1$ is adopted, we have $f_x(\theta)|_{\theta=0^\circ}=129.500$. Therefore, the obtained results are incorrect in general if $a=\lambda_1$ is adopted. In addition, if $a=0.9\lambda_1$ and $a=1.1\lambda_1$ are adopted, we have $f_x(\theta)|_{\theta=0^\circ}=-0.543$ and $f_x(\theta)|_{\theta=0^\circ}=-0.547$, respectively. Besides, the exact value is $f_x(\theta)|_{\theta=0^\circ}=-0.546$. Therefore, we can get the accurate results if $a=0.9\lambda_1$ or $a=1.1\lambda_1$ is adopted. From Fig. 8, it is seen that the dependence of the functions $f_y(\theta)$ to the used size "a" is not significant.

It is proved by computation that the critical value $a=\lambda_1$ will solely give an improper (or singular) solution for the component p_1.

It is necessary to explain one point in detail. There must have an exact solution for the two degenerate scale critical values

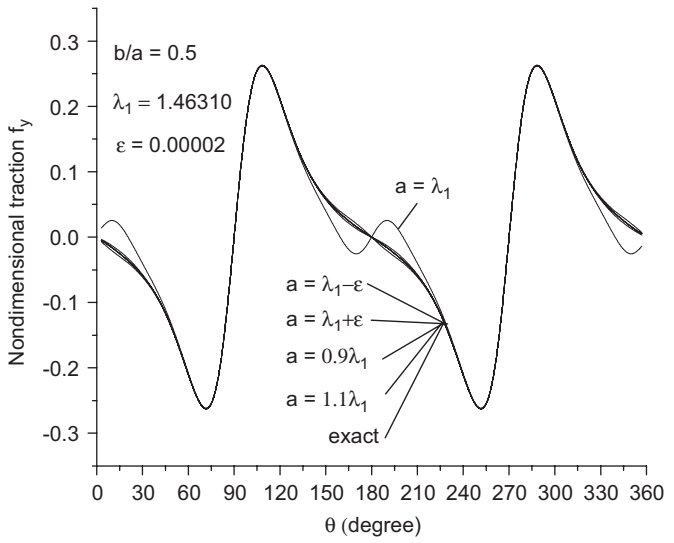

Fig. 8. Non-dimensional boundary tractions $f_y(\theta)$ on the elliptic boundary under the conditions: (a) $b/a = 0.5$; (b) the assumed displacements from Eq. (64); (c) for five cases: $a = \lambda_1 - \varepsilon$, $a = \lambda_1$, $a = \lambda_1 + \varepsilon$, $a = 0.9\lambda_1$ and $a = 1.1\lambda_1$ ($\lambda_1 = 1.46310$, $\varepsilon = 0.00002$) (see Fig. 4(a) and Eq. (67)).

$a = \lambda_{1(\text{exact})}$ and $a = \lambda_{2(\text{exact})}$. If we could find the real value of $a = \lambda_{1(\text{exact})}$, then there must have $\det(\mathbf{U}) = 0$, at $a = \lambda_{1(\text{exact})}$. In this case, the algebraic equation does not have solution. In a real computation, we can only get a value $a = \lambda_1$ that is a sufficient approximation to $a = \lambda_{1(\text{exact})}$. For example, we have got the following estimation $1.4631019781 < \lambda_{1(\text{exact})} < 1.4631019782$ from computation. In this case, even one takes a sufficient approximate value, for example, $a = \lambda_1 = 1.4631019781$, there still has $\det(\mathbf{U}) \neq 0$. In this case, the algebraic equation has a solution. Finally, it is pointed out that in all cited numerical examples, the used $a = \lambda_1$ and $a = \lambda_2$ are some approximate values for $a = \lambda_{1(\text{exact})}$ and $a = \lambda_{2(\text{exact})}$.

Example 4.2. As shown by Fig. 8, the critical value $a = \lambda_1$ does not give the component p_2 an improper solution in the previous example. In the present example, it will be shown that critical value $a = \lambda_2$ will give the component p_2 an improper solution.

In the example, we propose the following complex potentials

$$\phi(z) = \mathrm{i}Q_0 \ln z, \quad \psi(z) = \mathrm{i}\kappa Q_0 \ln z, \tag{68}$$

where Q_0 is a loading that has a dimension of force. Therefore, from Eqs. (4)–(6), the stresses and the displacements can be evaluated

$$\sigma_x + \sigma_y = 4Q_0 \,\mathrm{Re}\,\frac{\mathrm{i}}{z}, \quad \sigma_y - \sigma_x + 2\mathrm{i}\sigma_{xy} = 2Q_0\mathrm{i}\left(-\frac{\bar{z}}{z^2} + \frac{\kappa}{z}\right), \tag{69}$$

$$2G(u + \mathrm{i}v) = Q_0\mathrm{i}\left(2\kappa \ln |z| + \frac{z}{\bar{z}}\right). \tag{70}$$

In addition, from Eqs. (5) and (68) the amount of the resultant force in y-direction applied on the boundary will be $2\pi(\kappa + 1)Q_0$. The relevant loading condition is shown in Fig. 4(b).

In this example, computations for five cases, $a = \lambda_2 - \varepsilon$, $a = \lambda_2$, $a = \lambda_2 + \varepsilon$, $a = 0.9\lambda_2$, and $a = 1.1\lambda_2$ ($\lambda_2 = 1.21576$, $\varepsilon = 0.00002$) are performed. Under the same condition as mentioned in the Example 4.1, the computed results for tractions are expressed as follows:

$$p_1 = f_x(\theta)\frac{\pi(\kappa + 1)Q_0}{a}, \quad p_2 = f_y(\theta)\frac{\pi(\kappa + 1)Q_0}{a}$$
(tractions at the boundary points,
$x = a\cos\theta, \quad y = b\cos\theta$). (67)

The computed results for $f_x(\theta)$, and $f_y(\theta)$ are plotted in Figs. 9–11. For comparison, the exact result from Eq. (69) is also shown in the figures.

Contrary to the previous case, from Fig. 9 it is seen that the dependence of the functions $f_x(\theta)$ to the used size "a" is not significant. In this example, the most significant feature of the critical value can be seen from Figs. 10 and 11. In fact, the exact values for $f_y(\theta)$ are varying within the range $-1.074 \leqslant f_y(\theta) \leqslant -0.091$ (Fig. 11). However, if $a = \lambda_2$ is adopted, we have $f_y(\theta)|_{\theta=0^\circ} = 29.251$. Therefore, the obtained results are

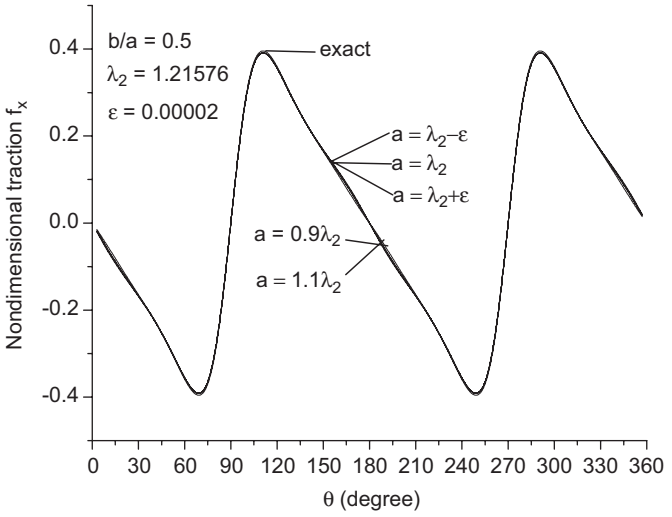

Fig. 9. Non-dimensional boundary tractions $f_x(\theta)$ on the elliptic boundary under the conditions: (a) $b/a = 0.5$; (b) the assumed displacements from Eq. (68); (c) for five cases: $a = \lambda_2 - \varepsilon$, $a = \lambda_2$, $a = \lambda_2 + \varepsilon$, $a = 0.9\lambda_2$ and $a = 1.1\lambda_2$ ($\lambda_2 = 1.21576$, $\varepsilon = 0.00002$) (see Fig. 4(b) and Eq. (67)).

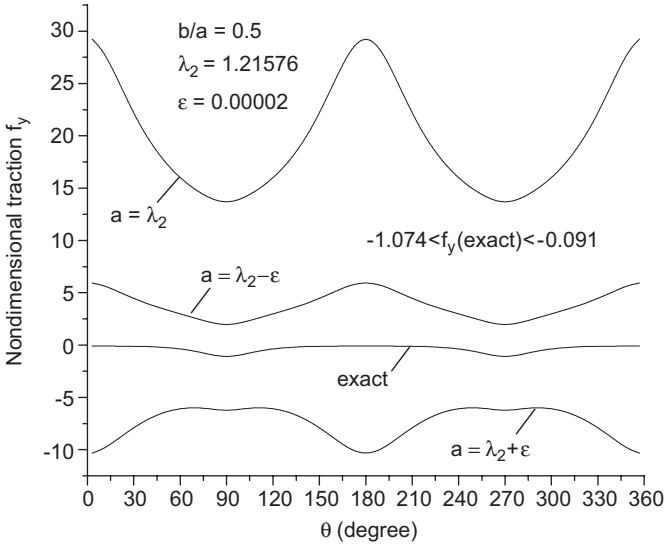

Fig. 10. Non-dimensional boundary tractions $f_y(\theta)$ on the elliptic boundary under the conditions: (a) $b/a = 0.5$; (b) the assumed displacements from Eq. (68); (c) for three cases: $a = \lambda_2 - \varepsilon$, $a = \lambda_2$, $a = \lambda_2 + \varepsilon$ ($\lambda_2 = 1.21576$, $\varepsilon = 0.00002$) (see Fig. 4(b) and Eq. (67)).

incorrect in general if $a=\lambda_2$ is adopted. In addition, if $a=0.9\lambda_2$ and $a=1.1\lambda_2$ are adopted, we have $f_y(\theta)|_{\theta=90^\circ}=-1.088$ and $f_y(\theta)|_{\theta=90^\circ}=-1.089$, respectively. In addition, the exact value is $f_y(\theta)|_{\theta=90^\circ}=-1.091$. Also, the three curves from (a) exact solution, (b) $a=0.9\lambda_2$, and (c) $a=1.1\lambda_2$ are merged into one curve (see Fig. 11). Therefore, we can get the accurate results for tractions if $a=0.9\lambda_2$ or $a=1.1\lambda_2$ is adopted.

As in the first example, we find that the second critical value $a=\lambda_2$ will solely give an improper solution for the component p_2.

Example 4.3. The third example is devoted to a triangle configuration with no symmetry condition (Fig. 4(c)).

Similar to the ellipse case, in the case of using the kernel $U_{ij}^{*1}(\xi,x,a)$, the obtained critical values are expressed as

$$\lambda_1=f_1\left(\frac{b}{a}\right),\quad \lambda_2=f_2\left(\frac{b}{a}\right). \tag{53}$$

Besides, in the case of using the kernel $U_{ij}^{*2}(\xi,x,a)$, the obtained scale critical values are expressed as

$$\lambda_1=g_1\left(\frac{b}{a}\right),\quad \lambda_2=g_2\left(\frac{b}{a}\right). \tag{61}$$

The computed results for $\lambda_1=f_1(b/a)$, $\lambda_2=f_2(b/a)$, $\lambda_1=g_1(b/a)$, and $\lambda_2=g_2(b/a)$ are listed in Table 3.

For two critical values $a=\lambda_1=1.575118$ and $a=\lambda_2=1.205902$ (for $b/a=0.5$ case using the kernel $U_{ij}^{*1}(\xi,x,a)$), the non-trivial solution for $\tilde{p}_n$ for the homogenous Eq. (50) can be found in a similar manner. The computed results for tractions under the condition $f_x(s/L)|_{s=0}=1$ are expressed as follows:

$$p_1=f_x\left(\frac{s}{L}\right),\quad p_2=f_y\left(\frac{s}{L}\right)\quad \text{(tractions at the boundary points, for } a=\lambda_1=1.575118 \text{ case)}, \tag{71}$$

$$p_1=g_x\left(\frac{s}{L}\right),\quad p_2=g_y\left(\frac{s}{L}\right)\quad \text{(tractions at the boundary points, for } a=\lambda_2=1.205902 \text{ case)}. \tag{72}$$

In Eqs. (71) and (72), the coordinate for "s" is starting at a point of the right side of triangle, and "L" is defined by $L=2(a+b+\sqrt{a^2+b^2})$ (Fig. 4(c)). The computed results for $f_x(s/L)$, $f_y(s/L)$, $g_x(s/L)$ and $g_y(s/L)$ are plotted in Figs. 12 and 13, which represent the non-trivial solution for the homogeneous Eq. (50). It is seen from the computed results that both components are not vanishing (or $p_1\neq 0, p_2\neq 0$), simply because of the unsymmetrical geometry of the triangle. In the case of using $a=\lambda_1=1.575118$, the component $f_x(s/L)$ is dominant in the magnitude. However, in the case of using $a=\lambda_2=1.205902$, the component $g_y(s/L)$ is dominant in the magnitude.

In the example, we propose the following complex potentials

$$\phi(z)=Q_0\ln z,\quad \psi(z)=-\kappa Q_0\ln z, \tag{64}$$

where Q_0 is a loading that has a dimension of force. Similar to the Example 4.1, the exact values for displacements and tractions along the notch contour can be found. From Eqs. (5) and (64) the amount of the resultant force in x-direction applied on the interior boundary will be $2\pi(\kappa+1)Q_0$. The relevant loading condition is

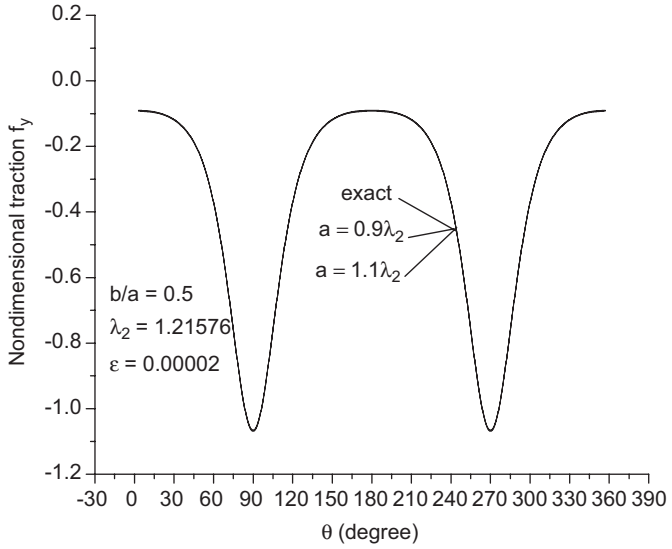

Fig. 11. Non-dimensional boundary tractions $f_y(\theta)$ on the elliptic boundary under the conditions: (a) $b/a=0.5$; (b) the assumed displacements from Eq. (68); (c) for two cases: $a=0.9\lambda_2$ and $a=1.1\lambda_2$ ($\lambda_2=1.21576$) (see Fig. 4(b) and Eq. (67)).

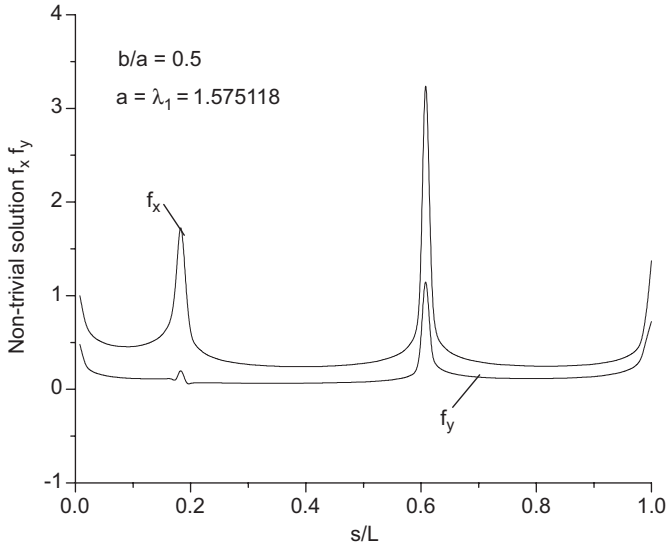

Fig. 12. Non-trivial solution for the boundary tractions $f_x(x/L)$ and $f_y(x/L)$ on the triangle notch under the conditions: (a) $b/a=0.5$; (b) $a=\lambda_1=1.575118$ (see Fig. 4(c) and Eq. (71)).

Table 3
Two critical values for the triangle notch case: (1) $a=\lambda_1=f_1(b/a)$ and $a=\lambda_2=f_2(b/a)$ in the case of using the kernel $U_{ij}^{*1}(\xi,x,a)$ (see Eq. (34)), (2) $a=\lambda_1=g_1(b/a)$ and $a=\lambda_2=g_2(b/a)$ in the case of using the kernel $U_{ij}^{*2}(\xi,x,a)$(see Eq. (37)), within the range $0.1\leqslant b/a\leqslant 1.0$ (see Fig. 4(c))

b/a	0.1	0.2	0.3	0.4	0.5	0.6	0.7	0.8	0.9	1.0
f_1	2.31587	2.07019	1.87397	1.71154	1.57512	1.45968	1.36181	1.27848	1.20720	1.14569
f_2	1.45054	1.38270	1.32073	1.26219	1.20590	1.15127	1.09801	1.04609	0.99572	0.94727
g_1	3.05740	2.73305	2.47400	2.25957	2.07946	1.92706	1.79785	1.68783	1.59373	1.51254
g_2	1.91499	1.82543	1.74362	1.66634	1.59202	1.51990	1.44958	1.38105	1.31455	1.25057

shown in Fig. 4(c) approximately. Same numerical solution technique mentioned in the Example 4.1 is used in the present example.

As mentioned above, there are two critical values $a = \lambda_1 = 1.575118$ and $a = \lambda_2 = 1.205902$ in the case of $b/a = 0.5$.

In the numerical examination, computations for five cases, $a = \lambda_1 - \varepsilon$, $a = \lambda_1$, $a = \lambda_1 + \varepsilon$, $a = 0.9\lambda_1$, and $a = 1.1\lambda_1$ ($\lambda_1 = 1.575118$, $\varepsilon = 0.000002$) are performed. The computed results for tractions are expressed as follows:

$$p_1 = f_x\left(\frac{s}{L}\right)\frac{\pi(\kappa+1)Q_0}{a}, \quad p_2 = f_y\left(\frac{s}{L}\right)\frac{\pi(\kappa+1)Q_0}{a}$$
(tractions at the boundary points for tractions on the boundary). (73)

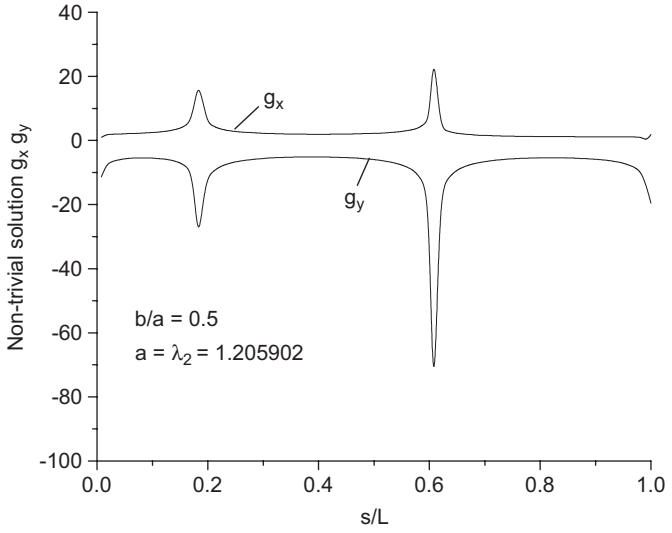

Fig. 13. Non-trivial solution for the boundary tractions $g_x(x/L)$ and $g_y(x/L)$ on the triangle notch under the conditions: (a) $b/a = 0.5$; (b) $a = \lambda_2 = 1.205902$ (see Fig. 2(c) and Eq. (72)).

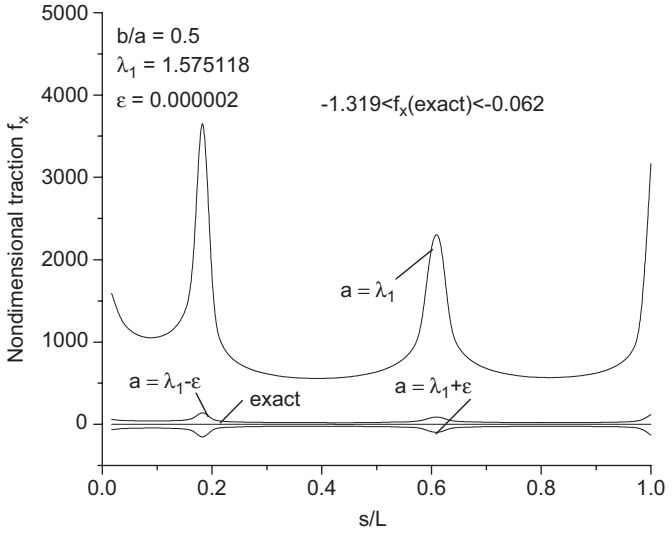

Fig. 14. Non-dimensional boundary tractions $f_x(s/L)$ on the triangle boundary under the conditions: (a) $b/a = 0.5$; (b) the assumed displacements from Eq. (64); (c) for three cases: $a = \lambda_1 - \varepsilon$, $a = \lambda_1$ and $a = \lambda_1 + \varepsilon$ ($\lambda_1 = 1.575118$, $\varepsilon = 0.000002$) (see Fig. 4(c) and Eq. (73)).

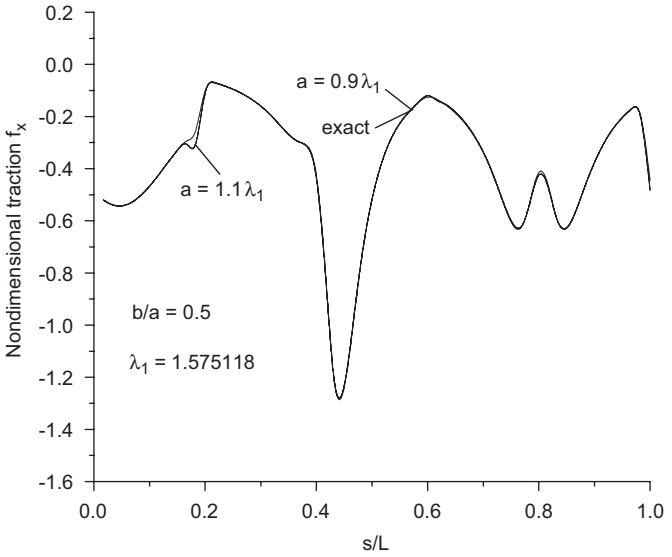

Fig. 15. Non-dimensional boundary tractions $f_x(s/L)$ on the triangle boundary under the conditions: (a) $b/a = 0.5$; (b) the assumed displacements from Eq. (64); (c) for two cases: $a = 0.9\lambda_1$ and $a = 1.1\lambda_1$ ($\lambda_1 = 1.575118$) (see Fig. 4(c) and Eq. (73)).

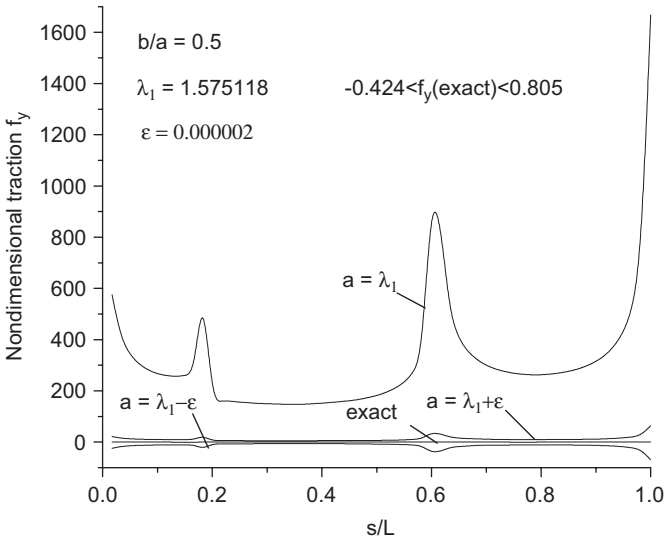

Fig. 16. Non-dimensional boundary tractions $f_y(s/L)$ on the triangle boundary under the conditions: (a) $b/a = 0.5$; (b) the assumed displacements from Eq. (64); (c) for three cases: $a = \lambda_1 - \varepsilon$, $a = \lambda_1$ and $a = \lambda_1 + \varepsilon$ ($\lambda_1 = 1.575118$, $\varepsilon = 0.000002$) (see Fig. 4(c) and Eq. (73)).

The computed results for $f_x(x/L)$, and $f_y(y/L)$ are plotted in Figs. 14–17. For comparison, the exact result from Eqs. (5) and (64) is also shown in the figures.

Some particular features can be found from the present example. If the used size "a" is equal to or near to the critical value, for example,$a = \lambda_1 - \varepsilon$, $a = \lambda_1$, $a = \lambda_1 + \varepsilon$, the computed results for $f_x(x/L)$ and $f_y(y/L)$ are generally incorrect. However, if the used size "a" takes the value $a = 0.9\lambda_1$ or $a = 1.1\lambda_1$, the computed results for $f_x(x/L)$ and $f_y(y/L)$ are sufficient accurate.

Similarly, computations for five cases, $a = \lambda_2 - \varepsilon$, $a = \lambda_2$, $a = \lambda_2 + \varepsilon$, $a = 0.9\lambda_2$, and $a = 1.1\lambda_2$ ($\lambda_2 = 1.205902$, $\varepsilon = 0.000002$) are performed. Since no new finding was found in computation, the computed results need not to describe.

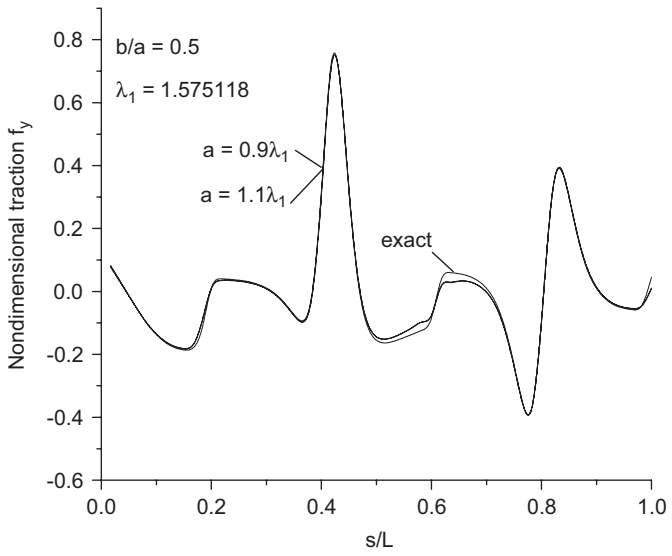

Fig. 17. Non-dimensional boundary tractions $f_y(s/L)$ on the triangle boundary under the conditions: (a) $b/a = 0.5$; (b) the assumed displacements from Eq. (64); (c) for two cases: $a = 0.9\lambda_1$ and $a = 1.1\lambda_1$ ($\lambda_1 = 1.575118$) (see Fig. 4(c) and Eq. (73)).

4.3. Technique for avoiding the improper solution

From mentioned numerical examples, a technique for avoiding the improper solutions is introduced. In the technique, one must not use the dimension "a" too near to the two critical values $a = \lambda_1$ and $a = \lambda_2$. It is suggested to use $a \geqslant 1.1\lambda_1$ or $a \leqslant 0.9\lambda_2$. Validity of this approach is easily seen from the computed results in the three numerical examples, particularly, from Figs. 7, 11, 15 and 17. This technique can be used when the λ_1 and λ_2 values can be obtained from other references.

If the λ_1 and λ_2 values have not known beforehand, the normal scale can be assumed in the following way. It is known for circular hole case that, $a = b = 1$ is a degenerate scale. In the case of rigid line (or $b = 0$), from Eq. (54) we have, $a = \lambda_1 = 2\exp(1/2\kappa) = 2.64038$ and $a = \lambda_2 = 2\exp(-1/2\kappa) = 1.51493$. Therefore, three is no degenerate scale larger than 5. In this case, for an elliptic notch it is sufficient to take $b = 5$ and $a = 5/\beta$ (β defined by $\beta = b/a$) as the normal scale.

In most cases, a very simple technique for finding the normal scale was suggested [5]. For example, if one meet a computation with the size $a = 2$ m, one simply replaces the dimension $a = 2$ m by $a = 200$ cm, then the numerical instability in the BIE solution will disappear. In this case, one does not need to perform a computation for the critical value.

5. Conclusions

The regularity condition at infinity in the exterior problem is important for the formulation of BIE. The relevant analysis depends on two factors: (a) the representation form of the displacement–stress field for the fundamental field and (b) the loading condition on the notch. A new kernel $U_{ij}^{*1}(\xi, x)$ has been found, which satisfies the regularity condition in general case of non-equilibrated loadings on the contour. For elliptic notch case, the degenerate scale based on the usage of $U_{ij}^{*1}(\xi, x)$ and numerical solution coincides with that from exact solution [11].

As mentioned above, it is complicated to analyze the degenerate scale problem in the form of the integral equation shown by Eq. (45). After discretization, the critical value can be evaluated from the property of the influence matrix. In addition to the critical value, the non-trivial solution can also be found numerically.

The computed results for tractions on the contour for BIE based on the usage of the suggested kernel $U_{ij}^{*1}(\xi, x)$ coincide with those from exact solution when the normal scale is used.

Acknowledgment

The project is supported by the National Natural Science Foundation of China.

References

[1] Rizzo FJ. An integral equation approach to boundary value problems in classical elastostatics. Quart J Appl Math 1967;25:83–95.
[2] Cruse TA. Numerical solutions in three-dimensional elastostatics. Int J Solids Struct 1969;5:1259–74.
[3] Brebbia CA, Tells JCF, Wrobel LC. Boundary element techniques—theory and application in engineering. Heidelberg: Springer; 1984.
[4] Cheng AHD, Cheng DS. Heritage and early history of the boundary element method. Eng Anal Boundary Elem 2005;29:286–302.
[5] Chen JT, Lin SR, Chen KH. Degenerate scale problem when solving Laplace's equation by BEM and its treatment. Int J Numer Methods Eng 2005;62: 233–61.
[6] Chen JT, Lee CF, Chen IL, Lin JH. An alternative method for degenerate scale problems in boundary element methods for the two-dimensional Laplace equation. Eng Anal Boundary Elem 2002;26:559–69.
[7] Chen JT, Lin JH, Kuo SR, Chiu YP. Analytical study and numerical experiments for degenerate scale problem in boundary element method using degenerate kernels and circulants. Eng Anal Boundary Elem 2001;25:819–28.
[8] He WJ, Ding HJ, Hu HC. Non-equivalence of the conventional boundary integral formulation and its elimination for plane elasticity problems. Comput Struct 1996;59:1059–62.
[9] He WJ, Ding HJ, Hu HC. Degenerate scales and boundary element analysis of two-dimensional potential and elasticity problems. Comput Struct 1996; 60:155–8.
[10] Vodička R, Mantič V. On solvability of a boundary integral equation of the first kind for Dirichlet boundary value problems in plane elasticity. Comput Mech 2007, doi:10.1007//s00466-007-0202-x, in press.
[11] Chen JT, Kuo SR, Lin JH. Analytical study and numerical experiments for degenerate scale problems in the boundary element method of two-dimensional elasticity. Int J Numer Methods Eng 2002;54:1669–81.
[12] Vodička R, Mantič V. On invertibility of elastic single-layer potential operator. J Elasticity 2004;74:147–73.
[13] Chen YZ, Wang ZX, Lin XY. Numerical examination for degenerate scale problem for ellipse-shpaed region in BIE. Int J Numer Methods Eng 2007; 71:1208–30.
[14] Muskhelishvili NI. Some basic problems of mathematical theory of elasticity. The Netherlands: Noordhoof; 1953.
[15] Buecker HF. Field singularities and related integral representation. In: Sih GC, editor. Mechanics of fracture, vol. 1. Noordhoff: Leyden; 1973. p. 239–314.
[16] Chen YZ. Analysis of L-integral and theory of the derivative stress field in plane elasticity. Int J Solids Struct 2003;40:3589–602.